Inorganic Chemistry

Article

pubs.acs.org/IC

# Quaternary Germanides $RE_4Mn_2InGe_4$ (RE = La–Nd, Sm, Gd–Tm, Lu)

Anton O. Oliynyk, Stanislav S. Stoyko, and Arthur Mar*

Department of Chemistry, University of Alberta, Edmonton, Alberta, Canada T6G 2G2

Supporting Information

**ABSTRACT:** The quaternary germanides $RE_4Mn_2InGe_4$ (RE = La–Nd, Sm, Gd–Tm, Lu) have been prepared by arc-melting reactions of the elements and annealing at 800 °C and represent the second example of the $RE_4M_2InGe_4$ series previously known only for M = Ni. Single-crystal X-ray diffraction studies conducted on the earlier RE members of $RE_4Mn_2InGe_4$ confirmed that they adopt the monoclinic $Ho_4Ni_2InGe_4$-type structure [space group $C2/m$, $a$ = 16.646(2)–15.9808(9) Å, $b$ = 4.4190(6)–4.2363(2) Å, $c$ = 7.4834(10)–7.1590(4) Å, $\beta$ = 106.893(2)–106.304(1)° in the progression of RE from La to Gd]. The covalent framework contains Mn-centered tetrahedra and $Ge_2$ dimers that build up $[Mn_2Ge_4]$ layers, which are held weakly together by four-coordinate In atoms and outline tunnels filled by the RE atoms. This bonding picture is supported by band-structure calculations. An alternative description based on Ge-centered trigonal prisms reveals that $RE_4Mn_2InGe_4$ is closely related to $RE_2InGe_2$. The electrical resistivity behavior of $Pr_4Mn_2InGe_4$ is similar to that of $Pr_2InGe_2$.

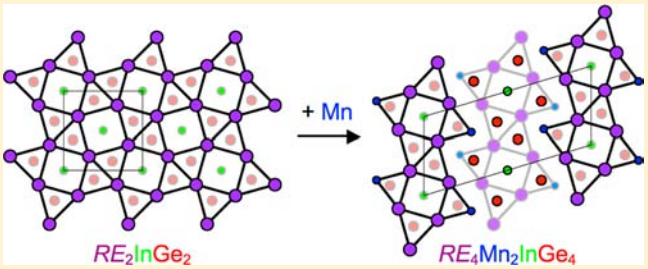


## INTRODUCTION

Ternary rare-earth transition-metal germanides RE–M–Ge form a large class of compounds that exhibit a rich variety of structures and physical properties; they have been especially well investigated for systems containing a first-row or later d-block element.[1,2] Ternary germanides are also known in which the M component is extended to include p-block metalloids from groups 13 and 14. Within the RE–In–Ge system, there exist several ternary phases,[3−11] the most common being $RE_2InGe_2$, which forms for many RE members.[3−6] The presence of two metalloids with similar electronegativities in these compounds leads to interesting heteroatomic and homoatomic bonding networks in their structures. Some of these compounds were initially discovered in the course of experiments intended to promote the crystal growth of ternary rare-earth transition-metal germanides. Through the use of a molten metal (such as Al, Ga, or In) behaving as a reactive flux, however, ternary metalloid-containing germanides as well as quaternary phases containing both d- and p-block components were obtained instead. In this way, the series $RE_4Ni_2InGe_4$ (RE = Dy, Ho, Er, Tm),[12] $RE_7Co_4InGe_{12}$ (RE = Dy, Ho, Yb),[13] and $Yb_3AuIn_3Ge_2$[14] were identified as new quaternary phases in the RE–M–In–Ge system (where M = d-block element). On the other hand, a fourth series, $RE_7Ni_{5-x}In_6Ge_{3+x}$ (RE = La–Nd, Sm), has been prepared simply through arc melting of the elements.[15,16] The combination of magnetically active species (from both the rare-earth and transition-metal components) and relatively complex crystal structures leads to potentially diverse physical properties for these quaternary germanides. There has also been some discussion in the literature on whether the flux-formed germanides represent thermodynamically stable phases in their phase diagrams.[6] In this regard, it is helpful to attempt the preparation of these complex germanides in the absence of a flux.

We present here the synthesis of quaternary germanides $RE_4Mn_2InGe_4$, which are manganese-containing analogues of the $RE_4Ni_2InGe_4$ series, and their structural characterization by powder and single-crystal X-ray diffraction. The large range of RE substitution permits elucidation of structural trends within this series. We highlight the close structural relationship between $RE_4M_2InGe_4$ (M = Mn, Ni) and $RE_2InGe_2$, which apparently has not been explicitly described previously. Band-structure calculations were performed to evaluate the bonding in $RE_4Mn_2InGe_4$.

## EXPERIMENTAL SECTION

**Synthesis.** Starting materials were freshly filed RE pieces (RE = La–Nd, Sm, Gd–Tm, Lu; 99.9%, Hefa), Mn powder (99.96%, Alfa-Aesar), In shot (99.999%, Cerac), and Ge pieces (99.9999%, Alfa-Aesar). Mixtures with the nominal composition "$RE_4Mn_2InGe_4$" were prepared from these elements, cold-pressed into pellets, and melted three times in a Centorr 5TA tri-arc furnace on a water-cooled copper hearth under an argon atmosphere. The weight loss after arc melting was less than 1%. The arc-melted ingots were then sealed within evacuated fused-silica tubes and annealed at 800 °C for 12 days, followed by quenching in cold water. The products were characterized by powder X-ray diffraction (XRD) patterns, collected with Cu $K\alpha_1$ radiation on an Inel diffractometer equipped with a curved position-sensitive detector (CPS 120). Qualitative analysis of the XRD patterns, with use of the program *Powder Cell* to compare with theoretical patterns,[17] revealed that the title compounds were formed in conjunction with $RE_2InGe_2$, $REMn_2Ge_2$, REMnGe, and $RE_{11}Ge_{10}$ as

Received: May 10, 2013
Published: July 1, 2013

   dx.doi.org/10.1021/ic401171v | Inorg. Chem. 2013, 52, 8264–8271

Table 1. Cell Parameters for $RE_4Mn_2InGe_4$ (RE = La−Nd, Sm, Gd−Lu)[a]

| compound | $a$ (Å) | $b$ (Å) | $c$ (Å) | $\beta$ (deg) | $V$ (Å$^3$) |
|---|---|---|---|---|---|
| $La_4Mn_2InGe_4$ | 16.666(1) | 4.4252(5) | 7.5023(6) | 106.958(4) | 529.2(1) |
| $Ce_4Mn_2InGe_4$ | 16.464(2) | 4.3724(6) | 7.3899(6) | 106.743(4) | 509.4(2) |
| $Pr_4Mn_2InGe_4$ | 16.367(1) | 4.3472(5) | 7.3523(6) | 106.876(5) | 500.6(1) |
| $Nd_4Mn_2InGe_4$ | 16.299(4) | 4.333(1) | 7.335(2) | 106.848(7) | 495.8(4) |
| $Sm_4Mn_2InGe_4$ | 16.112(2) | 4.2739(9) | 7.229(1) | 106.536(6) | 477.2(2) |
| $Gd_4Mn_2InGe_4$ | 16.018(2) | 4.2427(7) | 7.1732(6) | 106.358(4) | 467.8(5) |
| $Tb_4Mn_2InGe_4$ | 15.921(4) | 4.203(2) | 7.120(2) | 106.154(6) | 457.6(5) |
| $Dy_4Mn_2InGe_4$ | 15.857(2) | 4.1900(6) | 7.0938(5) | 106.146(7) | 452.7(2) |
| $Ho_4Mn_2InGe_4$ | 15.773(2) | 4.1661(5) | 7.0549(6) | 106.103(5) | 445.4(2) |
| $Er_4Mn_2InGe_4$ | 15.720(2) | 4.1488(7) | 7.0345(8) | 106.027(4) | 441.0(2) |
| $Tm_4Mn_2InGe_4$ | 15.648(2) | 4.1296(6) | 6.9990(8) | 105.996(6) | 434.8(2) |
| $Lu_4Mn_2InGe_4$ | 15.578(3) | 4.101(1) | 6.959(1) | 105.974(6) | 427.4(3) |

[a]Refined from powder XRD data.

Table 2. Crystallographic Data for $RE_4Mn_2InGe_4$ (RE = La−Nd, Sm, Gd)

| formula | $La_4Mn_2In_{0.945(2)}Ge_4$ | $Ce_4Mn_2In_{0.927(2)}Ge_4$ | $Pr_4Mn_2In_{0.921(2)}Ge_4$ | $Nd_4Mn_2In_{0.881(4)}Ge_4$ | $Sm_4Mn_2In_{0.904(3)}Ge_4$ | $Gd_4Mn_2In_{0.866(3)}Ge_4$ |
|---|---|---|---|---|---|---|
| formula mass (amu) | 1064.38 | 1066.93 | 1068.94 | 1078.24 | 1104.98 | 1128.56 |
| space group | $C2/m$ (No. 12) | $C2/m$ (No. 12) | $C2/m$ (No. 12) | $C2/m$ (No. 12) | $C2/m$ (No. 12) | $C2/m$ (No. 12) |
| $a$ (Å) | 16.646(2) | 16.4357(6) | 16.3401(11) | 16.249(3) | 16.093(2) | 15.9808(9) |
| $b$ (Å) | 4.4190(6) | 4.3652(2) | 4.3470(3) | 4.3313(7) | 4.2718(6) | 4.2363(2) |
| $c$ (Å) | 7.4834(10) | 7.3742(3) | 7.3425(5) | 7.3185(12) | 7.2124(10) | 7.1590(4) |
| $\beta$ (deg) | 106.893(2) | 106.6390(10) | 106.7210(10) | 106.813(2) | 106.458(2) | 106.3040(10) |
| $V$ (Å$^3$) | 526.72(12) | 506.91(4) | 499.49(6) | 493.05(14) | 475.51(11) | 465.17(4) |
| $Z$ | 2 | 2 | 2 | 2 | 2 | 2 |
| $\rho_{calcd}$ (g cm$^{-3}$) | 6.711 | 6.990 | 7.107 | 7.263 | 7.717 | 8.057 |
| $T$ (K) | 173(2) | 173(2) | 173(2) | 173(2) | 173(2) | 173(2) |
| crystal dimens (mm) | 0.09 × 0.06 × 0.03 | 0.14 × 0.05 × 0.05 | 0.09 × 0.03 × 0.03 | 0.11 × 0.04 × 0.03 | 0.07 × 0.04 × 0.04 | 0.09 × 0.05 × 0.02 |
| radiation | graphite monochromated Mo K$\alpha$, $\lambda$ = 0.71073 Å | | | | | |
| $\mu$(Mo K$\alpha$) (mm$^{-1}$) | 31.32 | 33.60 | 35.36 | 37.04 | 41.31 | 45.42 |
| transmn factors | 0.167−0.484 | 0.067−0.309 | 0.179−0.580 | 0.123−0.454 | 0.175−0.379 | 0.088−0.438 |
| 2$\theta$ limits | 5.12−66.48° | 5.18−66.36° | 5.20−66.40° | 5.24−66.40° | 5.28−66.30° | 5.32−66.46° |
| data collected | $-25 \le h \le 25$, $-6 \le k \le 6$, $-11 \le l \le 11$ | $-24 \le h \le 25$, $-6 \le k \le 6$, $-11 \le l \le 11$ | $-24 \le h \le 24$, $-6 \le k \le 6$, $-11 \le l \le 11$ | $-24 \le h \le 24$, $-6 \le k \le 6$, $-10 \le l \le 11$ | $-24 \le h \le 24$, $-6 \le k \le 6$, $-10 \le l \le 10$ | $-24 \le h \le 24$, $-6 \le k \le 6$, $-10 \le l \le 11$ |
| no. of data collected | 3733 | 3628 | 3612 | 3642 | 3390 | 3319 |
| no. of unique data, including $F_o^2 < 0$ | 1099 ($R_{int}$ = 0.028) | 1063 ($R_{int}$ = 0.018) | 1052 ($R_{int}$ = 0.025) | 1029 ($R_{int}$ = 0.029) | 994 ($R_{int}$ = 0.033) | 978 ($R_{int}$ = 0.026) |
| no. of unique data, with $F_o^2 > 2\sigma(F_o^2)$ | 989 | 1028 | 942 | 912 | 896 | 887 |
| no. of variables | 37 | 37 | 37 | 37 | 37 | 37 |
| $R(F)$ for $F_o^2 > 2\sigma(F_o^2)$[a] | 0.020 | 0.017 | 0.020 | 0.026 | 0.022 | 0.018 |
| $R_w(F_o^2)$[b] | 0.042 | 0.038 | 0.047 | 0.066 | 0.052 | 0.037 |
| GOF | 1.05 | 1.16 | 1.07 | 1.07 | 1.07 | 1.10 |
| $(\Delta\rho)_{max}$, $(\Delta\rho)_{min}$ (e Å$^{-3}$) | 1.93, −1.12 | 1.68, −1.25 | 2.62, −1.09 | 3.97, −1.40 | 3.34, −1.40 | 1.82, −1.11 |

[a]$R(F) = \sum||F_o| - |F_c||/\sum|F_o|$. [b]$R_w(F_o^2) = [\sum[w(F_o^2 - F_c^2)^2]/\sum wF_o^4]^{1/2}$; $w^{-1} = [\sigma^2(F_o^2) + (Ap)^2 + Bp]$, where $p = [\max(F_o^2,0) + 2F_c^2]/3$.

the most common accompanying phases (Table S1 in the Supporting Information). Cell parameters were refined with use of the *CSD* suite of programs[18] and are listed in Table 1. Energy-dispersive X-ray (EDX) analysis was performed on selected crystals on a JEOL JSM-6010LA scanning electron microscope, operated with an accelerating voltage of 20 kV and an acquisition time of 70 s. For five of the members of the $RE_4Mn_2InGe_4$ series (RE = La, Ce, Pr, Tm, Lu), these analyses gave experimental compositions (38−39% RE, 18−19% Mn, 7−8% In, and 35−36% Ge) that agree reasonably well with the fully stoichiometric formula (36.4% RE, 18.2% Mn, 9.1% In, and 36.4% Ge). As discussed below, there is evidence for a slight substoichiometry in indium, corresponding to the formula $RE_4Mn_2In_{0.9}Ge_4$, but the expected composition (36.7% RE, 18.3% Mn, 8.2% In, and 36.7% Ge) does not deviate sufficiently to permit EDX analysis, which is typically precise to only a few percent, to provide definitive support. For the remaining samples, overlap of RE with Mn or Ge peaks in the EDX spectra precluded quantitative analysis.

**Structure Determination.** Sufficiently large single crystals of $RE_4Mn_2InGe_4$, which were gray and irregularly shaped, were available for RE = La−Nd, Sm, and Gd. Intensity data were collected on a Bruker D8 diffractometer equipped with a SMART APEX II CCD area detector and a Mo K$\alpha$ radiation source, using $\omega$ scans at 6−8 different $\phi$ angles with a frame width of 0.3° and an exposure time of 12 s per frame. Face-indexed numerical absorption corrections were applied. Structure solution and refinement were carried out with use of the *SHELXTL* (version 6.12) program package.[19] The centrosymmetric monoclinic space group $C2/m$ was chosen on the basis of Laue symmetry, systematic absences, and intensity statistics. Direct methods revealed the initial atomic positions corresponding to the $Ho_4Ni_2InGe_4$-type structure.[12] Atomic coordinates were standardized


dx.doi.org/10.1021/ic401171v | *Inorg. Chem.* 2013, 52, 8264−8271

Table 3. Atomic Coordinates and Equivalent Isotropic Displacement Parameters (Å) for $RE_4Mn_2InGe_4$ (RE = La−Nd, Sm, Gd)

| | $La_4Mn_2In_{0.945(2)}Ge_4$ | $Ce_4Mn_2In_{0.927(2)}Ge_4$ | $Pr_4Mn_2In_{0.921(2)}Ge_4$ | $Nd_4Mn_2In_{0.881(4)}Ge_4$ | $Sm_4Mn_2In_{0.904(3)}Ge_4$ | $Gd_4Mn_2In_{0.866(3)}Ge_4$ |
|---|---|---|---|---|---|---|
| RE1 in 4*i* (*x*, 0, *z*) | | | | | | |
| *x* | 0.34869(2) | 0.34856(1) | 0.34779(2) | 0.34837(2) | 0.34697(2) | 0.34642(2) |
| *z* | 0.07052(4) | 0.07032(3) | 0.07133(4) | 0.07190(5) | 0.07277(4) | 0.07408(4) |
| $U_{eq}$ | 0.0074(1) | 0.0065(1) | 0.0067(1) | 0.0071(1) | 0.0061(1) | 0.0064(1) |
| RE2 in 4*i* (*x*, 0, *z*) | | | | | | |
| *x* | 0.58252(2) | 0.58211(1) | 0.58169(2) | 0.58085(2) | 0.58089(2) | 0.58057(2) |
| *z* | 0.36528(4) | 0.36473(3) | 0.36612(4) | 0.36504(5) | 0.36627(4) | 0.36699(4) |
| $U_{eq}$ | 0.0073(1) | 0.0066(1) | 0.0066(1) | 0.0067(1) | 0.0062(1) | 0.0064(1) |
| Mn in 4*i* (*x*, 0, *z*) | | | | | | |
| *x* | 0.21679(4) | 0.21744(4) | 0.21840(5) | 0.21888(7) | 0.21956(6) | 0.22018(5) |
| *z* | 0.62018(10) | 0.61982(8) | 0.61982(11) | 0.61892(15) | 0.61928(13) | 0.61883(12) |
| $U_{eq}$ | 0.0083(1) | 0.0071(1) | 0.0074(2) | 0.0069(2) | 0.0067(2) | 0.0069(2) |
| In in 2*a* (0, 0, 0) | | | | | | |
| occupancy | 0.945(2) | 0.927(2) | 0.921(2) | 0.881(4) | 0.904(3) | 0.866(3) |
| $U_{eq}$ | 0.0107(2) | 0.0092(1) | 0.0099(2) | 0.0103(2) | 0.0087(2) | 0.0092(2) |
| Ge1 in 4*i* (*x*, 0, *z*) | | | | | | |
| *x* | 0.06228(3) | 0.06276(2) | 0.06309(3) | 0.06336(5) | 0.06377(4) | 0.06384(4) |
| *z* | 0.64873(7) | 0.65019(6) | 0.65145(8) | 0.65175(10) | 0.65308(9) | 0.65464(8) |
| $U_{eq}$ | 0.0079(1) | 0.0067(1) | 0.0069(1) | 0.0068(2) | 0.0064(1) | 0.0068(1) |
| Ge2 in 4*i* (*x*, 0, *z*) | | | | | | |
| *x* | 0.20235(3) | 0.20111(3) | 0.19878(4) | 0.19749(5) | 0.19588(4) | 0.19381(4) |
| *z* | 0.25755(8) | 0.25494(6) | 0.25157(8) | 0.24909(11) | 0.24653(9) | 0.24366(8) |
| $U_{eq}$ | 0.0089(1) | 0.0082(1) | 0.0080(1) | 0.0075(2) | 0.0073(1) | 0.0074(1) |

Table 4. Interatomic Distances (Å) in $RE_4Mn_2InGe_4$ (RE = La−Nd, Sm, Gd)

| | $La_4Mn_2In_{0.945(2)}Ge_4$ | $Ce_4Mn_2In_{0.927(2)}Ge_4$ | $Pr_4Mn_2In_{0.921(2)}Ge_4$ | $Nd_4Mn_2In_{0.881(4)}Ge_4$ | $Sm_4Mn_2In_{0.904(3)}Ge_4$ | $Gd_4Mn_2In_{0.866(3)}Ge_4$ |
|---|---|---|---|---|---|---|
| RE1−Ge1 (×2) | 3.1117(5) | 3.0685(3) | 3.0467(4) | 3.0265(6) | 2.9876(5) | 2.9582(4) |
| RE1−Ge2 | 3.1423(7) | 3.1010(5) | 3.0877(6) | 3.0872(9) | 3.0346(8) | 3.0140(6) |
| RE1−Ge2 (×2) | 3.2278(5) | 3.1720(3) | 3.1442(5) | 3.1227(7) | 3.0727(6) | 3.0418(4) |
| RE1−Mn | 3.4465(9) | 3.4030(6) | 3.3805(9) | 3.3738(12) | 3.3320(11) | 3.3167(9) |
| RE1−In (×2) | 3.5038(4) | 3.4594(2) | 3.4546(3) | 3.4333(5) | 3.4110(4) | 3.3944(2) |
| RE1−Mn (×2) | 3.5907(7) | 3.5469(5) | 3.5281(7) | 3.5262(9) | 3.4625(8) | 3.4302(6) |
| RE2−Ge1 (×2) | 3.1481(5) | 3.1112(3) | 3.0939(5) | 3.0852(7) | 3.0397(6) | 3.0179(4) |
| RE2−Ge2 (×2) | 3.2320(5) | 3.1861(4) | 3.1651(5) | 3.1517(7) | 3.1044(6) | 3.0723(4) |
| RE2−Ge1 (×2) | 3.2489(5) | 3.2087(3) | 3.1877(5) | 3.1669(7) | 3.1333(6) | 3.1041(5) |
| RE2−Mn | 3.3109(9) | 3.2637(6) | 3.2384(8) | 3.2222(12) | 3.1833(11) | 3.1573(9) |
| RE2−Mn (×2) | 3.3223(6) | 3.2944(5) | 3.2848(6) | 3.2805(9) | 3.2504(8) | 3.2336(7) |
| RE2−In (×2) | 3.4726(4) | 3.4264(2) | 3.4158(3) | 3.3945(5) | 3.3596(4) | 3.3388(2) |
| Mn−Ge2 (×2) | 2.6106(6) | 2.5886(4) | 2.5908(5) | 2.5904(8) | 2.5699(7) | 2.5662(6) |
| Mn−Ge1 | 2.6420(9) | 2.6151(7) | 2.6141(9) | 2.6067(13) | 2.5868(12) | 2.5822(10) |
| Mn−Ge1 | 2.6539(10) | 2.6265(7) | 2.6296(10) | 2.6272(14) | 2.6062(11) | 2.5992(10) |
| In−Ge1 (×2) | 3.0933(6) | 3.0401(4) | 3.0217(6) | 3.0123(8) | 2.9613(7) | 2.9274(6) |
| In−Ge2 (×2) | 3.3597(7) | 3.3017(4) | 3.2418(6) | 3.1995(9) | 3.1500(8) | 3.0988(6) |
| Ge1−Ge1 | 2.5636(10) | 2.5585(8) | 2.5609(10) | 2.5549(15) | 2.5536(13) | 2.5552(11) |

with use of the program *STRUCTURE TIDY*.[20] Structure refinements were straightforward except that the displacement parameters for the In site were consistently elevated compared to the other sites. Successive refinements indicated partial occupancy for the In site [ranging from 0.944(3) in the La member to 0.864(7) in the Gd member], in contrast to full occupancies for all remaining sites [0.99(1)−1.02(1)]. Similar observations were previously made for the $RE_4Ni_2InGe_4$ series, for which the occupancy of the In site was 0.96 or greater.[12] It is possible that the elevated displacement parameters are intrinsic, given the unusual coordination geometry of this In site; establishing the existence of a homogeneity range in In will require further synthetic experiments. For brevity, the idealized formula $RE_4Mn_2InGe_4$ is used in subsequent discussion but the nonstoichiometric formula $RE_4Mn_2In_{1-x}Ge_4$ is retained in the crystallographic tables. Crystal data and further experimental details are given in Table 2. Final values of the positional and displacement parameters are given in Table 3, and selected interatomic distances are given in Table 4. Further data in the form of crystallographic information files (CIFs) are available as the Supporting Information or may be obtained from Fachinformationszentrum Karlsruhe, Abt. PROKA, 76344 Eggenstein-Leopoldshafen, Germany (CSD 426119−426124).

**Band-Structure Calculations.** Tight-binding linear muffin tin orbital band-structure calculations were performed on a fully stoichiometric $La_4Mn_2InGe_4$ model within the local density and atomic sphere approximations with use of the Stuttgart *TB-LMTO-ASA* program (version 4.7).[21] The basis set consisted of La 6s/6p/5d/4f, Mn 4s/4p/3d, In 5s/5p/5d/4f, and Ge 4s/4p/4d orbitals, with the La 6p, In 5d/4f, and Ge 4d orbitals being downfolded. Integrations in reciprocal space were carried out with an improved tetrahedron method over 554 irreducible *k* points within the first Brillouin zone.

**Electrical Resistivity Measurement.** A block-shaped crystal of $Pr_4Mn_2InGe_4$, whose identity was confirmed by EDX analysis (39% Pr,


dx.doi.org/10.1021/ic401171v | *Inorg. Chem.* 2013, 52, 8264−8271

18% Mn, 7% In, and 36% Ge), was mounted for standard four-probe electrical resistivity measurements between 2 and 300 K on a Quantum Design Physical Property Measurement System (PPMS) equipped with an alternating-current transport controller (model 7100). The current was 100 $\mu$A, and the frequency was 16 Hz.

## RESULTS AND DISCUSSION

Quaternary germanides $RE_4M_2InGe_4$ were previously known only for M = Ni[12] and have been extended here to include M = Mn. The RE substitution is limited to the later members for $RE_4Ni_2InGe_4$ (RE = Dy−Tm) but spans through all of the typically trivalent members in $RE_4Mn_2InGe_4$ (RE = La−Nd, Sm, Gd−Tm, Lu), with the unit cell volumes steadily decreasing as expected following the lanthanide contraction (Figure 1). This contrast is probably attributable to the

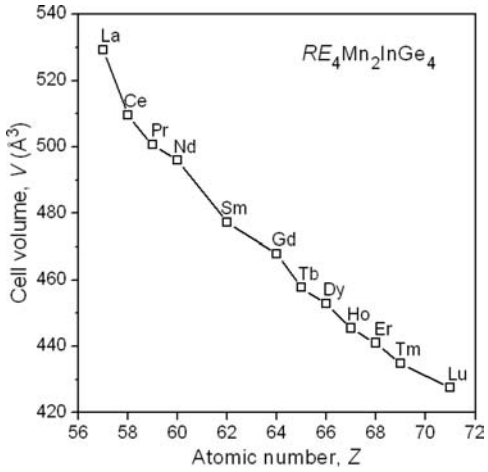


**Figure 1.** Plot of the unit cell volumes in $RE_4Mn_2InGe_4$.

different synthetic conditions used. The Ni-containing compounds were prepared through off-stoichiometric reactions with substantial excess of In at temperatures no higher than 1000 °C; stoichiometric reactions through induction melting or arc melting, but with no subsequent annealing step, were apparently unsuccessful.[12] On the other hand, the Mn-containing compounds were prepared by arc-melting stoichiometric mixtures of the elements followed by annealing at 800 °C. The arc-melting process assures that the melting points are exceeded and compound formation takes place upon cooling. The presence of considerable amounts of secondary phases after annealing implies that decomposition has probably occurred during equilibration, although we cannot rule out experimental errors such as the loss of small amounts of Mn during the cold-pressing of pellets. It seems likely that the $RE_4Ni_2InGe_4$ series can be extended to more RE members, perhaps through the use of arc melting/annealing instead of a flux technique, and that further $RE_4M_2InGe_4$ series can be prepared for other transition-metal components M. Further optimization of the synthesis of these compounds will require detailed elucidation of the phase diagrams, which are very complicated for these quaternary systems, where up to four phases can be present at equilbrium (Table S1 in the Supporting Information). Heat treatment at temperatures different from 800 °C may improve the sample purity. With the existence of these quaternary germanides now established, it is worthwhile to attempt flux growth to obtain crystals.

The germanides $RE_4Mn_2InGe_4$ adopt the monoclinic $Ho_4Ni_2InGe_4$-type structure.[12] If the RE atoms are assumed to participate in ionic interactions only, the remaining atoms form a covalent bonding network built from $MnGe_4$ tetrahedra, $InGe_4$ square planes, and $Ge_2$ dimers (Figure 2). The Mn-

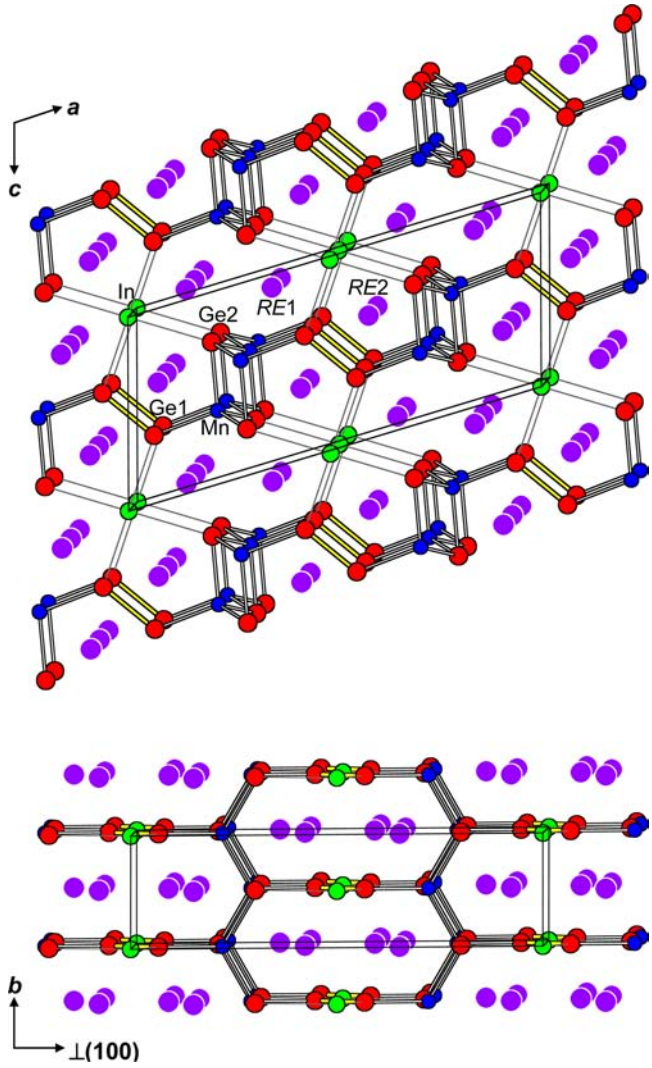


**Figure 2.** Structure of $RE_4Mn_2InGe_4$ highlighting the $[Mn_2InGe_4]$ covalent bonding network, viewed along the *b* (top) and *c* (bottom) directions. The large purple circles are RE atoms, the small blue circles are Mn atoms, the medium green circles are In atoms, and the medium red circles are Ge atoms.

centered tetrahedra share edges to form double chains $[Mn_2Ge_{4/2}]$ extending along the *b* direction; in turn, these chains are connected by the $Ge_2$ dimers along the *a* direction to form $[Mn_2Ge_4]$ layers that lie parallel to the *ab* plane. The In atoms in square-planar coordination serve to bridge these $[Mn_2Ge_4]$ layers together to form the three-dimensional network. The resulting framework delimits tunnels extending along the *b* and *c* directions within which the RE atoms are located. There are similarities to other germanides, such as $Yb_2Zn_3Ge_3$,[22] $La_4Mg_7Ge_6$,[23] and $(Sr_{1-x}Ca_x)_5In_3Ge_6$,[24] which are built from the same structural units but connected in different ways.

It is helpful to examine the coordination polyhedra of each site (Figure 3) to clarify the relationship of the quaternary $Ho_4Ni_2InGe_4$-type structure adopted by $RE_4M_2InGe_4$ (M = Mn, Ni) to the binary $Mg_5Si_6$-type structure[25,26] from which it


dx.doi.org/10.1021/ic401171v | Inorg. Chem. 2013, 52, 8264−8271

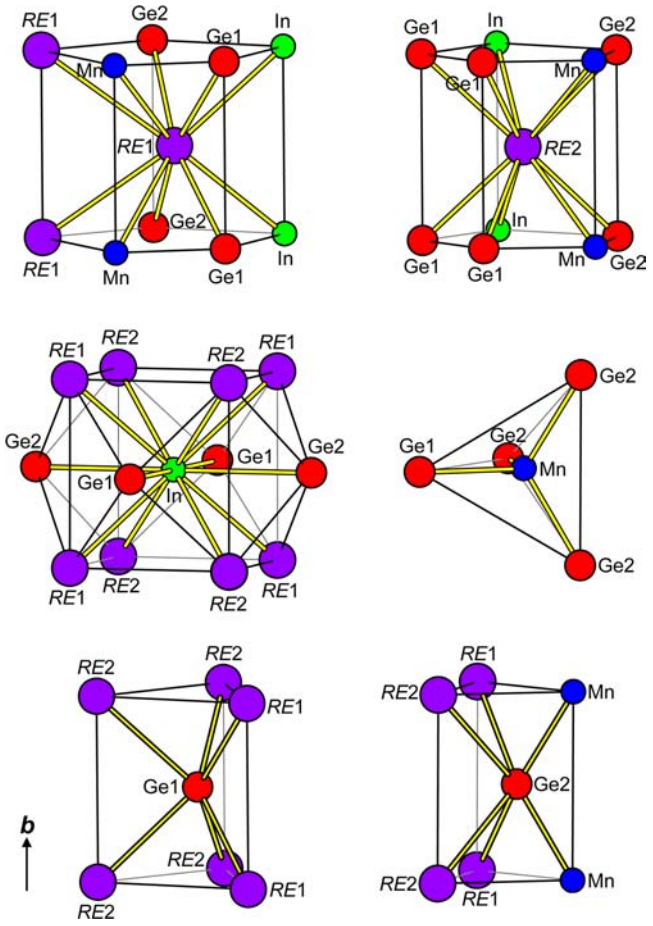


**Figure 3.** Coordination polyhedra in $RE_4Mn_2InGe_4$.

is derived as well as to the ternary or pseudoternary variants $Yb_4Mn_2Sn_5$[27] and $(Eu_{1-x}Ca_x)_4In_3Ge_4$ (Table 5).[28] The ordered

**Table 5. Comparison of Unit Cell Contents in $Mg_5Si_6$-Derived Structures**

| site | $Mg_5Si_6$ | $Yb_4Mn_2Sn_5$ | $(Eu_{1-x}Ca_x)_4In_3Ge_4$ | $RE_2M_2InGe_4$ |
|---|---|---|---|---|
| pentagonal prisms (4*i*, 4*i*) | 8 Mg | 8 Yb | 8 ($Eu_{1-x}Ca_x$) | 8 RE |
| tetrahedra (4*i*) | 4 Si | 4 Mn | 4 In | 4 M |
| tetragonal prisms (2*a*) | 2 Mg | 2 Sn | 2 In | 2 In |
| trigonal prisms (4*i*, 4*i*) | 8 Si | 8 Sn | 8 Ge | 8 Ge |

occupation of the six different sites within the parent $Mg_5Si_6$-type structure can be rationalized to a first approximation by size effects. The large electropositive components (alkaline- and rare-earth atoms) in these structures enter the sites with the highest CN, at the centers of pentagonal prisms. These prisms, which are augmented by additional capping atoms (not shown), figure prominently in $Mg_5Si_6$, and they are preserved in related binary Mg−Si and ternary Mg−Si−Al alloys.[29−31] The transition-metal components (Mn atoms in $Yb_4Mn_2Sn_5$; Mn or Ni atoms in $RE_4M_2InGe_4$) are generally the smallest and thus fill the tetrahedral sites, with the lowest CN. A noteworthy feature is the square-planar coordination of the metalloid components [Sn atoms in $Yb_4Mn_2Sn_5$; In atoms in $(Eu_{1-x}Ca_x)_4In_3Ge_4$ and $RE_4M_2InGe_4$]. The four surrounding atoms can be considered to cap the waists of a tetragonal prism (nearly a cube), reminiscent of what is found within the more prevalent $Mo_2FeB_2$-type structure.[32] The close relationship to these structures becomes apparent when coordination around the group 14 components is highlighted. As is common in many intermetallic germanides, the Ge atoms in $RE_4M_2InGe_4$ center trigonal prisms. If the $RE_4M_2InGe_4$ structure is portrayed in terms of these trigonal prisms ($RE_6$ around Ge1 and $RE_4M_2$ around Ge2), it is clearly seen to contain fragments of the tetragonal $Mo_2FeB_2$-type structure, adopted by ternary germanides $RE_2InGe_2$ for example (Figure 4).[3−6] In $RE_2InGe_2$,

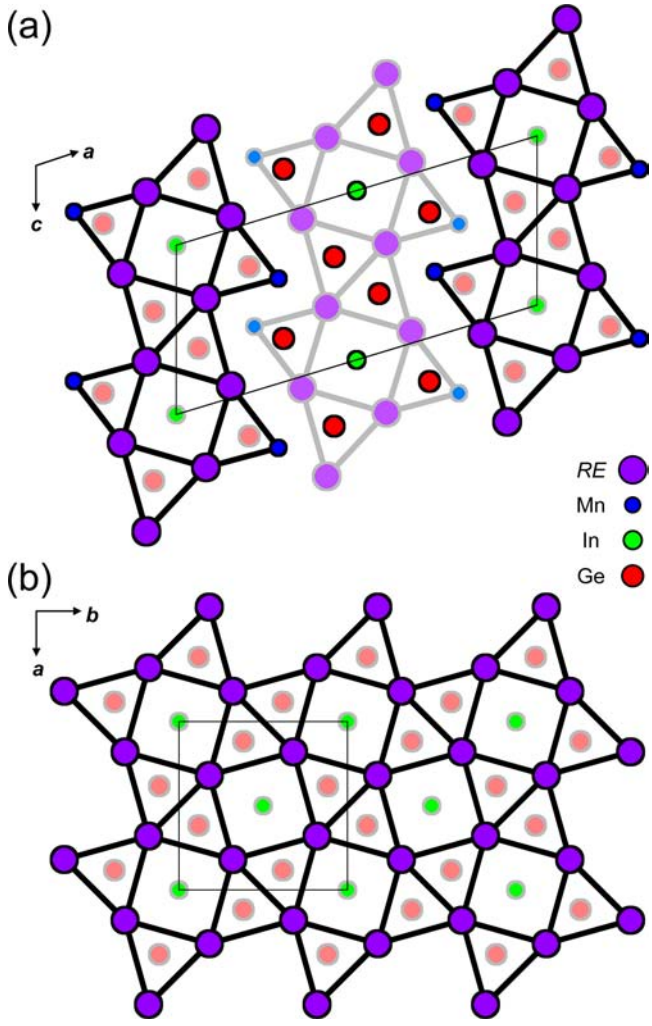


**Figure 4.** Comparison of (a) $RE_4Mn_2InGe_4$ ($Ho_4Ni_2InGe_4$-type) and (b) $RE_2InGe_2$ ($Mo_2FeB_2$-type) structures, represented in terms of Ge-centered trigonal prisms and In-centered tetragonal prisms. Dark and light lines distinguish between atoms displaced by half of the cell parameter along the viewing direction.

$3^2434$ nets of RE atoms are stacked along the *c* direction to form trigonal prisms occupied by Ge atoms and tetragonal prisms occupied by In atoms. In $RE_4M_2InGe_4$, the $3^2434$ nets are severed and the RE atoms in one of the corners of the trigonal prisms are replaced by M atoms to generate alternating slabs that are displaced by half the repeat parameter along the stacking direction, with the notches of each slab fitting into the grooves of the adjacent slabs.

The availability of single-crystal diffraction data for $RE_4Mn_2InGe_4$ (RE = La−Nd, Sm, Gd) allows structural trends to be examined more closely (Table 4). For reference, the sums


dx.doi.org/10.1021/ic401171v | *Inorg. Chem.* 2013, 52, 8264−8271

of Pauling metallic radii ($R_1$) are as follows: La−Ge, 2.93 Å; Gd−Ge, 2.86 Å; Mn−Ge, 2.42 Å; In−Ge, 2.66 Å; Ge−Ge, 2.48 Å.[33] The observed RE−Ge distances are within 0.1−0.2 Å of the expected values and decrease systematically with smaller RE. Concurrent with this contraction, the average Mn−Ge distance within the $MnGe_4$ tetrahedra does not vary much (2.58−2.63 Å) and the Ge1−Ge1 distance within the $Ge_2$ dimers is practically unchanged (2.56 Å), while the In−Ge distances shorten dramatically (from 3.09−3.36 Å in the La member to 2.93−3.10 Å in the Gd member) (Figure 5). The

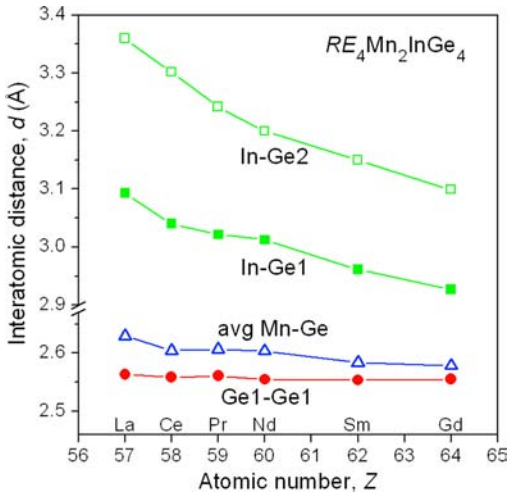


**Figure 5.** Plots of the Mn−Ge, In−Ge, and Ge−Ge distances in $RE_4Mn_2InGe_4$.

implication is that the Mn and Ge atoms define a relatively rigid framework, supporting the picture presented earlier of covalently bonded $[Mn_2Ge_2]$ layers bridged together via weaker bonds to In atoms. The bond length in the $Ge_2$ dimers in $RE_4Mn_2InGe_4$ is similar to those found in other polygermanides (typically 2.5−2.6 Å),[34−37] but the most relevant comparison is with $RE_4Ni_2InGe_4$, where it is also invariant (2.49 Å) with RE substitution.[12] The strengthening of the Ge−Ge bond as M is substituted with a later transition metal in $RE_4M_2InGe_4$ resembles the bond-making and bond-breaking effects seen in $AB_2X_2$ compounds with the $ThCr_2Si_2$-type structure.[38,39] The In−Ge distances, which separate into two inequivalent sets in $RE_4Mn_2InGe_4$, can be compared with those in $RE_2InGe_2$, where the In coordination is rigorously square planar; for a fixed RE, they are always longer in $RE_4Mn_2InGe_4$ (cf. 3.02−3.24 Å in $Pr_4Mn_2InGe_4$ vs 3.01 Å in $Pr_2InGe_2$).[3−6]

To evaluate the bonding in $RE_4Mn_2InGe_4$ in more detail, the electronic band structure has been calculated for the La member (Figure 6). From considerations of relative electronegativities (Pauling values of 1.1 for La, 1.6 for Mn, 1.8 for In, and 2.0 for Ge)[33] and directions of electron transfer, we expect to find mostly empty La states, partially filled Mn and In states, and mostly filled Ge states, as corroborated in the density of states (DOS) curve and its atomic projections. The three narrow bands lying lowest in energy (−10 to −7 eV) correspond essentially to the Ge 4s states and another narrow band at higher energy (centered at −5 eV) to the In 5s states. The broad manifold from −4 eV upward results from strong mixing of La 5d, Mn 3d, and Ge 4p states, with small contributions of the In 5p states. Empty La 5d states are found

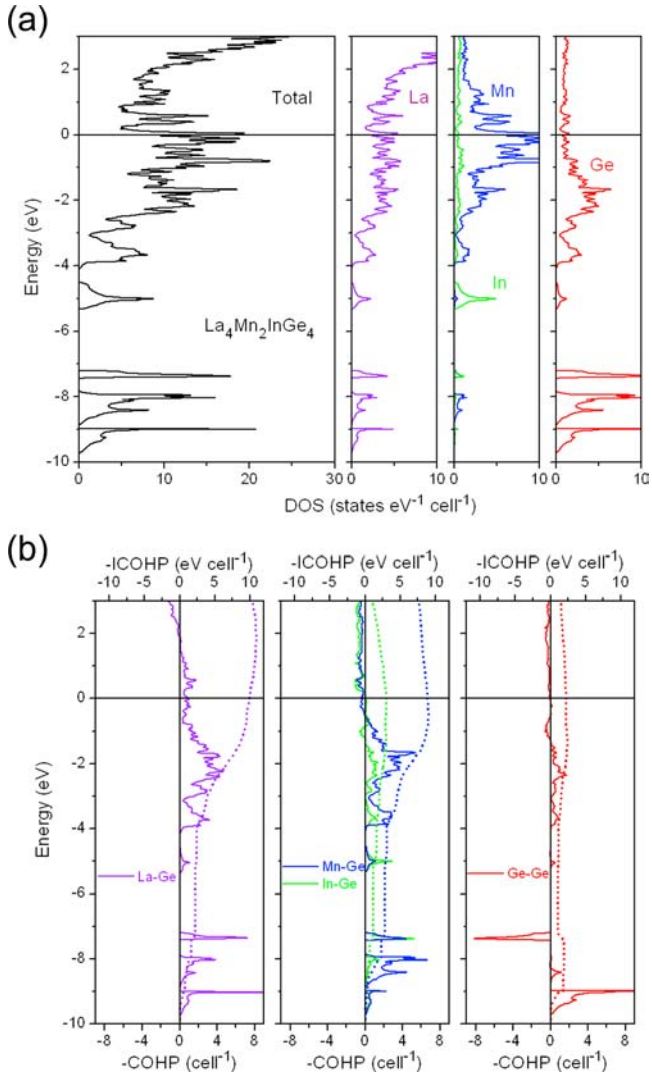


**Figure 6.** (a) DOS and its atomic projections for $La_4Mn_2InGe_4$. (b) COHP curves for La−Ge, Mn−Ge, In−Ge, and Ge−Ge contacts. The Fermi level is at 0 eV.

well above the Fermi level (0 eV). The DOS curve for $La_4Mn_2InGe_4$ resembles that for $Eu_2Ca_2In_3Ge_4$ except that the Mn 3d states are much more dominant near the Fermi level.[28] Consistent with the earlier discussion of bond distances, the crystal orbital Hamilton population (COHP) curves confirm the presence of La−Ge, Mn−Ge, and Ge−Ge bonding interactions resulting from the filling of most of the bonding states and of few of the antibonding states up to the Fermi level. The integrated COHP (−ICOHP) values are 0.9 eV/bond for La−Ge, 2.2 eV/bond for Mn−Ge, and 2.2 eV/bond for Ge−Ge contacts. The profile of the Ge−Ge COHP curve, which originates from the $Ge_2$ dimer in the crystal structure, captures the familiar pattern of molecular orbitals for a diatomic molecule: $\sigma_s$ and $\sigma_s$* levels (−9.5 and −7.5 eV, respectively), $\sigma_p$ and $\pi_p$ levels (−4 to −1.5 eV), and $\pi_p$* and $\sigma_p$* levels (−1.5 eV upward). The Fermi level cuts the merged $\pi_p$*/$\sigma_p$* states, consistent with a $(Ge_2)^{6-}$ species that is isoelectronic to a diatomic halogen molecule like $Br_2$ in which all but the $\sigma_p$* states are occupied. The In−Ge interactions around the unusual In environment are found to be weakly bonding, notwithstanding the long distances (−ICOHP values of 0.92 eV/bond for the 3.09 Å contacts and 0.58 eV/bond for the 3.36


dx.doi.org/10.1021/ic401171v | Inorg. Chem. 2013, 52, 8264−8271

Å contacts), similar to the situation in $Eu_2Ca_2In_3Ge_4$.[28] There is some evidence for In substoichiometry from the crystal structure determinations, but the decrease in the electron count would be small (from 45 $e^-$/f.u. in $La_4Mn_2InGe_4$ to 44.7 $e^-$/f.u. in $La_4Mn_2In_{0.9}Ge_4$) and the Fermi level would only be negligibly lowered by 0.02 eV.

The prediction of metallic behavior from the band structure of $La_4Mn_2InGe_4$, which can be assumed to be similar for other members of $RE_4Mn_2InGe_4$, is verified by electrical resistivity measurements on $Pr_4Mn_2InGe_4$ (Figure 7). The temperature

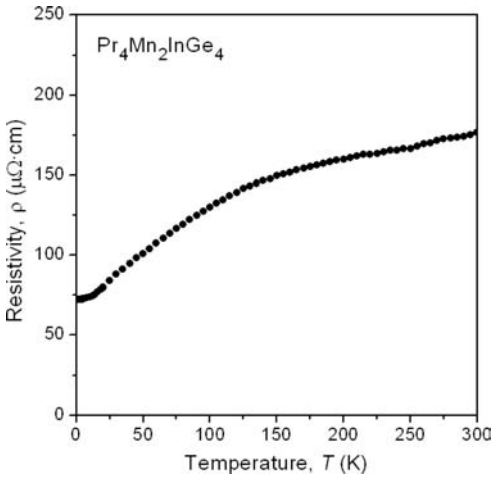


**Figure 7.** Electrical resistivity of $Pr_4Mn_2InGe_4$.

dependence exhibits distinct curvature, with two changes in the slope near 130 and 15 K. Similar kinks observed in the resistivity for $RE_2InGe_2$ (RE = Ce–Nd, Sm, Gd) are related to the development of long-range magnetic ordering, typically antiferromagnetism.[4,6] Given that the magnetic susceptibility of $Pr_2InGe_2$ undergoes an upturn near 15 K,[4] we speculate that the resistivity transition in $Pr_4Mn_2InGe_4$ at this same temperature originates from magnetic ordering of the Pr moments, whereas the transition at 130 K involves coupling with the Mn moments. Unfortunately, the arc-melting process did not yield single-phase samples required for magnetic measurements. It would be worthwhile to attempt the use of a flux, as was done for $RE_4Ni_2InGe_4$, even if it does not afford single-phase samples because magnetic measurements could still be made on selected large crystals of the desired compound.

## CONCLUSIONS

The $RE_4M_2InGe_4$ series, previously known only for M = Ni,[12] has now been extended to include M = Mn. It is probable that the isostructural series containing the intervening transition metals (M = Fe, Co) exist, and efforts are underway in our laboratory to prepare them. Analysis of the bonding favors a structural description involving $[Mn_2Ge_4]$ layers held weakly together by the In atoms, with RE atoms entering tunnels. However, we demonstrate that the structure of $RE_4M_2InGe_4$ can also be derived in a conceptually simple way from $RE_2InGe_2$ in which the introduction of M atoms into one of the RE sites in $RE_2InGe_2$ and cleavage of the $3^2434$ nets result in segregated slabs that are shifted with respect to each other. This alternative approach may prove helpful in the eventual interpretation of physical properties for $RE_4M_2InGe_4$ compounds, which are expected to be similar to those for $RE_2InGe_2$.

## ASSOCIATED CONTENT

### Supporting Information

X-ray crystallographic files in CIF format and a summary of phase analyses from powder XRD patterns. This material is available free of charge via the Internet at http://pubs.acs.org.

## AUTHOR INFORMATION

### Corresponding Author

*E-mail: arthur.mar@ualberta.ca.

### Notes

The authors declare no competing financial interest.

## ACKNOWLEDGMENTS

This work was supported by the Natural Sciences and Engineering Research Council of Canada.

## REFERENCES

(1) Salamakha, P. S.; Sologub, O. L.; Bodak, O. I. In *Handbook on the Physics and Chemistry of Rare Earths*; Gschneidner, K. A., Jr., Eyring, L., Eds.; Elsevier: Amsterdam, The Netherlands, 1999; Vol. *27*, pp 1–223.
(2) Salamakha, P. S. In *Handbook on the Physics and Chemistry of Rare Earths*; Gschneidner, K. A., Jr., Eyring, L., Eds.; Elsevier: Amsterdam, The Netherlands, 1999; Vol. *27*, pp 223–338.
(3) Zaremba, V. I.; Stępień-Damm, A.; Nichiporuk, G. P.; Tyvanchuk, Yu. B.; Kalychak, Ya. M. *Kristallografiya* **1998**, *43*, 13–16.
(4) Zaremba, V. I.; Kaczorowski, D.; Nychyporuk, G. P.; Rodewald, U. Ch.; Pöttgen, R. *Solid State Sci.* **2004**, *6*, 1301–1306.
(5) Zaremba, V. I.; Johrendt, D.; Rodewald, U. Ch.; Nychyporuk, G. P.; Pöttgen, R. *Solid State Sci.* **2005**, *7*, 998–1002.
(6) Tobash, P. H.; Lins, D.; Bobev, S.; Lima, A.; Hundley, M. F.; Thompson, J. D.; Sarrao, J. L. *Chem. Mater.* **2005**, *17*, 5567–5573.
(7) Guloy, A. M.; Corbett, J. D. *Inorg. Chem.* **1996**, *35*, 2616–2622.
(8) Nychyporuk, G.; Zaremba, V.; Kalychak, Ya.; Stępień-Damm, A.; Pietraszko, A. *J. Alloys Compd.* **2000**, *312*, 154–157.
(9) Mao, J.; Guloy, A. M. *J. Alloys Compd.* **2001**, *322*, 135–142.
(10) Mao, J.-G.; Goodey, J.; Guloy, A. M. *Inorg. Chem.* **2002**, *41*, 931–937.
(11) Zaremba, V. I.; Kaczorowski, D.; Nychyporuk, G. P.; Rodewald, U. Ch.; Heying, B.; Pöttgen, R. *Z. Anorg. Allg. Chem.* **2006**, *632*, 975–980.
(12) Salvador, J. R.; Kanatzidis, M. G. *Inorg. Chem.* **2006**, *45*, 7091–7099.
(13) Chondroudi, M.; Balasubramanian, M.; Welp, U.; Kwok, W.-K.; Kanatzidis, M. G. *Chem. Mater.* **2007**, *19*, 4769–4775.
(14) Chondroudi, M.; Peter, S. C.; Malliakas, C. D.; Balasubramanian, M.; Li, Q. A.; Kanatzidis, M. G. *Inorg. Chem.* **2011**, *50*, 1184–1193.
(15) Chumalo, N.; Nychyporuk, G. P.; Pavlyuk, V. V.; Pöttgen, R.; Kaczorowski, D.; Zaremba, V. I. *J. Solid State Chem.* **2010**, *183*, 2963–2967.
(16) Dominyuk, N.; Zaremba, V. I.; Pöttgen, R. *Z. Naturforsch., B.: J. Chem. Sci.* **2011**, *66*, 433–436.
(17) Kraus, W.; Nolze, G. *J. Appl. Crystallogr.* **1996**, *29*, 301–303.
(18) Akselrud, L. G.; Grin, Yu. N.; Zavalij, P. Yu.; Pecharsky, V. K.; Fundamenskii, V. S. Abstracts of Papers, 12th European Crystallographic Meeting, Moscow, USSR, Aug 20–29, 1989.
(19) Sheldrick, G. M. *SHELXTL*, version 6.12; Bruker AXS Inc.: Madison, WI, 2001.
(20) Gelato, L. M.; Parthé, E. *J. Appl. Crystallogr.* **1987**, *20*, 139–143.
(21) Tank, R.; Jepsen, O.; Burkhardt, A.; Andersen, O. K. *TB-LMTO-ASA Program*, version 4.7; Max Planck Institut für Festkörperforschung: Stuttgart, Germany, 1998.
(22) Grystiv, A.; Kaczorowski, D.; Rogl, P.; Tran, V.; Godart, C.; Gofryk, K.; Giester, G. *J. Phys.: Condens. Matter* **2005**, *17*, 385–397.
(23) Solokha, P.; De Negri, S.; Skrobanska, M.; Saccone, A.; Pavlyuk, V.; Proserpio, D. M. *Inorg. Chem.* **2012**, *51*, 207–214.
(24) You, T.-S.; Bobev, S. *J. Solid State Chem.* **2010**, *183*, 1258–1265.

(25) Zandbergen, H. W.; Andersen, S. J.; Jansen, J. *Science* **1997**, *277*, 1221−1225.
(26) Andersen, S. J.; Zandbergen, H. W.; Jansen, J.; Træholt, C.; Tundal, U.; Reiso, O. *Acta Mater.* **1998**, *46*, 3283−3298.
(27) Lei, X.-W.; Zhong, G.-H.; Li, M.-J.; Mao, J.-G. *J. Solid State Chem.* **2008**, *181*, 2448−2455.
(28) You, T.-S.; Tobash, P. H.; Bobev, S. *Inorg. Chem.* **2010**, *49*, 1773−1783.
(29) Andersen, S. J.; Marioara, C. D.; Frøseth, A.; Vissers, R.; Zandbergen, H. W. *Mater. Sci. Eng., A* **2005**, *390*, 127−138.
(30) van Huis, M. A.; Chen, J. H.; Zandbergen, H. W.; Sluiter, M. H. F. *Acta Mater.* **2006**, *54*, 2945−2955.
(31) van Huis, M. A.; Chen, J. H.; Sluiter, M. H. F.; Zandbergen, H. W. *Acta Mater.* **2007**, *55*, 2183−2199.
(32) Lukachuk, M.; Pöttgen, R. *Z. Kristallogr.* **2003**, *218*, 767−787.
(33) Pauling, L. *The Nature of the Chemical Bond*, 3rd ed.; Cornell University Press: Ithaca, NY, 1960.
(34) Choe, W.; Miller, G. J.; Levin, E. M. *J. Alloys Compd.* **2001**, *329*, 121−130.
(35) You, T.-S.; Bobev, S. *J. Solid State Chem.* **2010**, *183*, 2895−2902.
(36) Siggelkow, L.; Hlukhyy, V.; Fässler, T. F. *J. Solid State Chem.* **2012**, *191*, 76−89.
(37) Guo, S.-P.; Meyers, J. J.; Tobash, P. H.; Bobev, S. *J. Solid State Chem.* **2012**, *192*, 16−22.
(38) Hoffmann, R.; Zheng, C. *J. Phys. Chem.* **1985**, *89*, 4175−4181.
(39) Johrendt, D.; Felser, C.; Jepsen, O.; Andersen, O. K.; Mewis, A.; Rouxel, J. *J. Solid State Chem.* **1997**, *130*, 254−265.